

Loosely coherent searches for medium scale coherence lengths

Vladimir Dergachev^{1, 2, a}

¹Max Planck Institute for Gravitational Physics (Albert Einstein Institute), Callinstrasse 38, 30167 Hannover, Germany

²Leibniz Universität Hannover, D-30167 Hannover, Germany

The search for continuous gravitational waves demands computationally efficient algorithms that can handle highly non-linear parameter spaces. Loosely coherent algorithms establish upper limits and detect signals by analyzing families of templates as a single unit. We describe a new computationally efficient loosely coherent search intended for all-sky searches over medium scale coherence lengths (3–300 hours).

I. INTRODUCTION

In this paper we describe a novel *Loosely coherent* algorithm for detecting continuous almost monochromatic signals. Such signals are searched for in data collected by LIGO and Virgo gravitational wave interferometers. The data under analysis typically spans several months and searches [1–3] look for signals in the 20–2000 Hz frequency band.

Carrying out an all-sky search in this data typically requires several months of computation on large clusters. Large numbers of outliers are produced in initial stages due to imperfect data and must be dealt with in subsequent analysis. A successful search must combine efficient algorithms with top-notch technical implementation and excellent search execution.

In this paper we focus on the mathematical aspects of the newly implemented *Loosely coherent* code. Such description eases reuse of the algorithm in other searches, and can also serve as a reference for results papers using the new algorithm. We present validation results of a search pipeline built using this algorithm. A speed comparison to previous implementation shows more than 10x speedup.

The *Loosely coherent* algorithms were introduced in [4], as a general approach to signal detection based on exploring regions of parameter space at once. This contrasts with methods that focus on detecting a single template [5] and then iterate over template banks.

The algorithm implementing optimal statistic depends strongly on parameter space region morphology. For example, if the family of potential signals is only described by occupied bandwidth then the optimal statistic is a filter extracting this bandwidth followed by a power detector [4, 6]. On the other hand, long term drifts in the bandwidth window can be accommodated by dynamic programming algorithms which are fundamentally non-linear [3, 7, 8].

Some parameter spaces allow themselves to be split into regions for independent analysis without compromising efficiency. Such regions can be labeled by a representative signal waveform which can then be considered as

a “thick” template. This situation occurs in all-sky analysis where signal modulations are bounded, and usually no larger than $10^{-4} \cdot f$ at high signal frequencies f .

For example, one can split the bandwidth into 1/8 Hz bands which, effectively, creates a thick template bank. In practice, the partition is usually much finer and is done in all the search parameters. This is necessary to reduce memory footprint of practical implementation.

The signal families describing potential continuous gravitational wave signals generated by rotating neutron stars are complex. Even in the case of an isolated neutron star the incoming gravitational wave is expected to slowly drift in frequency, which is usually approximated with a linear term and sometimes quadratic term. By the time it reaches the detector the signal undergoes strong Doppler shifts from complex motion¹ of the detector around Earth rotation axis and along Earth orbit around the Sun. Relativistic effects come into play and the signals can be delayed due to gravitational field of Sun or other bodies [9].

The first implementation [4, 10] of a *Loosely coherent algorithm* computed power $P[f]$ as a function of frequency f . This function which can always be represented as a quadratic sum of input data $\{a_{t,f}\}$:

$$P[f] = \sum_{t_1, t_2} a_{t_1, f + \delta f(t_1)} a_{t_2, f + \delta f(t_2)}^* K_{t_1, t_2, f} \quad (1)$$

Here t_1 and t_2 denote times of frequency bins $\{a_{t,f}\}$ of short Fourier transforms (SFTs) of the data acquired by the detectors, f is the frequency of the desired signal, $\delta f(t)$ is the frequency shift of the signal received by the detectors.

This initial implementation focused on kernels $K_{t_1, t_2, f}$ with non-zero entries in a narrow diagonal band $|t_1 - t_2| < T$, where T depended on effective coherence length (usually a constant fraction of T) of the search. The input data was phase-corrected so that transformed data approximated a heterodyned signal that would have been received in Solar System Barycenter (SSB) frame[4]. The Lanza kernel was used that combined a low-pass filter and a power detector.

¹ Exact computation of phase corrections requires transcendental functions, see [9] for a computationally efficient approximation by polynomials

^a vladimir.dergachev@aei.mpg.de

This approach made sense because that *Loosely coherent* algorithm was used for followup of outliers produced by an algorithm that computed power in individual SFTs and required no phase corrections. The diagonal band was initially very short and then increased in subsequent stages.

However, as the width of diagonal band (and effective coherence length) was increased the speedup techniques would eventually become ineffective and the computational demands would scale quadratically with coherence length even for a single template, due to summation over two indices t_1, t_2 . Thus the algorithm was only practical for short coherence lengths (of a small multiple of SFT length) or when few templates would be searched compared to previous stages, such as during followup of outliers.

Long coherence lengths were explored with *Loosely coherent* algorithm designed for well-modeled signals [11], which scaled to coherence lengths of more than 10^6 s. While longer coherence length generally results in more sensitivity, the improvement in signal-to-noise ratio (SNR) scales only as forth root of increase in coherence length, while the size of parameter space scales as a forth power or faster.

Even though *Loosely coherent* algorithm for well-modeled signals was spending less than 1500 CPU cycles per template (amortized over the entire computation) [11] the forth power scaling made searches of large portions of the sky impractical on contemporary computer clusters.

This paper describes how to construct *Loosely coherent* algorithm for medium scale coherence lengths of 3–300 hours, assuming input data of 3600 s short Fourier transforms (SFTs).

II. LOOSELY COHERENT SUM

In order to construct a practical algorithm we must find an efficient way to compute the power sum in equation 1.

For long coherence length the power sum kernel $K_{t_1, t_2, f}$ must have a lot of non-zero terms making straightforward summation impractical. A well-known way [6] to speed up computation is to decompose total power into the sum of squares of coherent combinations of phase-corrected terms:

$$P[f] = \sum_{t_1} |CS[t_1, f]|^2 \quad (2)$$

with coherent sums CS given by

$$CS[t_1, f] = \sum_{t_2} w_{t_1 t_2} e^{i\phi(t_2)} a_{t_2, f + \delta f(t_2)} \quad (3)$$

The effective coherence length is then governed by the number of terms in the coherent sum CS and the computational load will scale linearly at this stage of the computation.

Both weights $w_{t_1 t_2}$ and phase corrections $\phi(t_2)$ vary over parameter space, however variation of weights is very gradual, so it makes sense to design our statistic assuming weights can be constant and precomputed over extended area. We will discuss weights in more detail in the subsequent section.

Because we are only interested in the absolute value of the coherent sum the variation of phase corrections over parameter space reduces to a second order difference operator:

$$\phi(t, p_1) - \phi(t, p_2) \sim \phi(t, p_1) - \phi(t_0, p_1) - \phi(t, p_2) + \phi(t_0, p_2) \quad (4)$$

Here p_1 and p_2 are two locations in the parameter space, t is some point of time for which we are interested in a phase correction, and t_0 is some fixed reference time, such as a midpoint of data being used in a single coherent sum. Because we are interested in power, the constant phase correction $\phi(t_0, p_1) - \phi(t_0, p_2)$ can be neglected.

The second order difference operator removes large portion of nonlinearity from Barycentric corrections, with the remainder described as relatively simple algebraic expression in functions of time and sky location [9].

Thus the differences are predictable based on local data. One straightforward way to take advantage of this is with an associative cache of previously computed coherent sums - if the expected phase differences are close enough we can reuse already computed result.

A more sophisticated approach being considered for future implementation is to use the explicit algebraic form of the differences [9] to compute power sums over a wider area on the sky. The algebraic form (or, at least, knowledge of the Lipschitz constant) is also essential for application of cubic algorithm [12], which performs global optimization.

III. COHERENT SUM WEIGHTS

We now address the question of how to pick weights when the noise level of underlying data $a_{t, f}$ varies. Because the weights in the different coherent sums can (and should be) chosen independently we will focus on a single coherent sum at a time.

To simplify notation we focus on a specific frequency f and introduce coherent sum elements z_i which are rescaled from $a_{t, f}$ so that the signal contributes the same amplitude and phase $Ae^{i\phi}$ to each z_i . The index i runs over individual SFTs used in the coherent sum. Because amplitude modulation needs to be backed out (discussed in the following section) the variance of noise component of z_i is expected to not be stationary.

We thus estimate power by computing absolute squared value of the weighted coherent sum CS

$$P = P_0 + |CS|^2 = P_0 + \left| \sum_{i=1}^N w_i z_i \right|^2 \quad (5)$$

where P_0 denotes contribution of other coherent sums, weights w_i are real and non-negative, while the coherent sum elements z_i are usually complex numbers. Normalization requires that the weights w_i should sum to 1.

Let us assume that the noise in z_i is uncorrelated. We will now find the optimal set of weights w_i that minimizes $U = \text{Var} |CS|^2$. This choice of the utility function is somewhat arbitrary, but the variance works well for common distributions like Gaussian or exponential and is easy to compute. It is not appropriate for quantifying spiky noise - this is best analyzed with other data quality techniques. In our case, we are interested in the behavior of the middle portion of the distribution.

Also, ideally, we should optimize the variance of the entire power sum P , but this would introduce dependence between weights of separate coherent sums when the coherent sums use overlapping stretches of data. In case of no overlap the coherent sums can be assumed independent and optimizing $\text{Var} P$ is the same as separately optimizing variance of each coherent sum.

We compute

$$\begin{aligned} U &= \text{Var} |CS|^2 = \text{Var} \left(\sum_{i,j=1}^N w_i w_j z_i \bar{z}_j \right) = \\ &= \sum_{i=1}^N w_i^4 \text{Var} |z_i|^2 + \\ &+ 4 \sum_{1 \leq i < j}^N w_i^2 w_j^2 (\mathbb{E}(\Re z_i)^2 \mathbb{E}(\Re z_j)^2 + \mathbb{E}(\Im z_i)^2 \mathbb{E}(\Im z_j)^2 + \\ &+ 2 \mathbb{E}(\Re z_i \Im z_i) \mathbb{E}(\Re z_j \Im z_j) - (\mathbb{E} z_i \mathbb{E} \bar{z}_j)^2) \end{aligned} \quad (6)$$

Let us consider the situation of background noise with no signal. In this case the phases would be randomly distributed and we can assume $\mathbb{E} \Re z_i = \mathbb{E} \Im z_i = 0$. Also randomness of phases implies $\mathbb{E}(\Re z_i)^2 = \mathbb{E}(\Im z_i)^2 = \mathbb{E} |z_i|^2 / 2$. Thus

$$U_{\text{bg}} = \sum_{i=1}^N w_i^4 \text{Var} |z_i|^2 + 2 \sum_{1 \leq i < j}^N w_i^2 w_j^2 \mathbb{E} |z_i|^2 \mathbb{E} |z_j|^2 \quad (7)$$

If z_i are Gaussian then $|z_i|^2$ is exponentially distributed and $\text{Var} |z_i|^2 = (\mathbb{E} |z_i|^2)^2$. Thus

$$\begin{aligned} U_{\text{Gauss bg}} &= \sum_{i=1}^N w_i^4 (\mathbb{E} |z_i|^2)^2 + 2 \sum_{1 \leq i < j}^N w_i^2 w_j^2 \mathbb{E} |z_i|^2 \mathbb{E} |z_j|^2 = \\ &= \left(\sum_{i=1}^N w_i^2 \mathbb{E} |z_i|^2 \right)^2 \end{aligned} \quad (8)$$

Thus for a Gaussian z_i with randomly distributed phases minimizing U is equivalent to minimizing $\sum_{i=1}^N w_i^2 \mathbb{E} |z_i|^2$. The optimum is easily found:

$$w_i = \frac{1}{\mathcal{N}} \frac{1}{\mathbb{E} |z_i|^2} = \frac{1}{\mathcal{N}} \frac{1}{\sqrt{\text{Var} |z_i|^2}} \quad (9)$$

Here \mathcal{N} is a suitable normalizing factor.

IV. POLARIZATION ANALYSIS

We will now derive explicit formulas for loosely coherent power sums.

Let us assume that the incoming gravitational wave signal is a monochromatic wave represented as [5]

$$\begin{aligned} h_+ &= A_+ \cos(\omega t + \phi) \cos(\epsilon) - A_\times \sin(\omega t + \phi) \sin(\epsilon) \\ h_\times &= A_+ \cos(\omega t + \phi) \sin(\epsilon) + A_\times \sin(\omega t + \phi) \cos(\epsilon) \end{aligned} \quad (10)$$

where $\epsilon = 2\psi$ describes orientation of the pulsar, ϕ is the initial signal phase, $\omega = 2\pi f$ is the pulsar gravitational wave frequency and $A_+ = h_0(1 + \cos^2(\iota))/2$ and $A_\times = h_0 \cos(\iota)$ are amplitudes.

The signal received by the detector is described by

$$s(t) = F_+(t)h_+ + F_\times(t)h_\times \quad (11)$$

where $F_+(t)$ and $F_\times(t)$ are time-varying amplitude response variables of the detector.

The input data consists of short Fourier transforms with coherence length small enough that one can assume that $F_+(t)$ and $F_\times(t)$ do not vary significantly.

The frequency bin $a_{t,f}$ of the SFT taken at time t can thus be described as

$$\begin{aligned} a_{t,f} &= n_{t,f} + F_+(t)(A_+ e^{i\Phi(t)} \cos(\epsilon) + A_\times i e^{i\Phi(t)} \sin(\epsilon)) + \\ &+ F_\times(t)(A_+ e^{i\Phi(t)} \sin(\epsilon) - A_\times i e^{i\Phi(t)} \cos(\epsilon)) = \\ &= n_{t,f} + h_0 e^{i\Phi(t)} (F_+(t)w'_1 + F_\times(t)w'_2) \end{aligned} \quad (12)$$

where $n_{t,f}$ is the detector noise. The variables w'_1 and w'_2 are complex amplitude parameters [11], they satisfy

$$\sqrt{|w'_1 + iw'_2|} + \sqrt{|w'_1 - iw'_2|} = 1 \quad (13)$$

The coherent power sum computed over SFTs taken at times t_1, \dots, t_N is

$$\text{PS} = \left| \sum_{i=1}^N w_i a_{t_i, f_i} e^{-i\Phi(t_i)} / (F_+(t_i)w'_1 + F_\times(t_i)w'_2) \right|^2 \quad (14)$$

where we used

$$z_i = a_{t_i, f_i} e^{-i\Phi(t_i)} / (F_+(t_i)w'_1 + F_\times(t_i)w'_2) \quad (15)$$

The division by amplitude response of the detector effectively increases noise level of SFTs at time of unfavorable orientation. Thus we expect the optimal weights to deweight these terms.

Assuming n_{t_i, f_i} are Gaussian the optimal weights computed in the previous section are:

$$w_i = |F_+(t_i)w'_1 + F_\times(t_i)w'_2|^2 / \mathbb{E} |n_{t_i, f_i}|^2 \quad (16)$$

The normalizing factor is

$$\mathcal{N} = \sum_{i=1}^n w_i \quad (17)$$

And thus the optimal power sum is

$$PS = \frac{1}{\mathcal{N}^2} \left| \sum_{i=1}^N a_{t_i, f_i} e^{-i\Phi(t_i)} \frac{F_+(t_i) \bar{w}'_1 + F_\times(t_i) \bar{w}'_2}{\mathbb{E} |n_{t_i, f_i}|^2} \right|^2 \quad (18)$$

The normalizing factor can be expressed as

$$\begin{aligned} \mathcal{N} = & \left(\sum_{i=1}^N F_+(t_i)^2 / \mathbb{E} |n_{t_i, f_i}|^2 \right) |w'_1|^2 + \\ & + \left(\sum_{i=1}^N F_\times(t_i)^2 / \mathbb{E} |n_{t_i, f_i}|^2 \right) |w'_2|^2 + \\ & + 2 \left(\sum_{i=1}^N F_\times(t_i) F_+(t_i) / \mathbb{E} |n_{t_i, f_i}|^2 \right) \Re(w'_1 \bar{w}'_2) \end{aligned} \quad (19)$$

Let us define two intermediate coherent sums CS_+ and CS_\times :

$$\begin{aligned} CS_+ &= \sum_{i=1}^N a_{t_i, f_i} e^{-i\Phi(t_i)} F_+(t_i) / \mathbb{E} |n_{t_i, f_i}|^2 \\ CS_\times &= \sum_{i=1}^N a_{t_i, f_i} e^{-i\Phi(t_i)} F_\times(t_i) / \mathbb{E} |n_{t_i, f_i}|^2 \end{aligned} \quad (20)$$

Then the power sum is expressed as

$$PS = \frac{1}{\mathcal{N}^2} (|CS_+|^2 |w'_1|^2 + |CS_\times|^2 |w'_2|^2 + 2\Re(CS_+ \overline{CS_\times} w'_2 \bar{w}'_1)) \quad (21)$$

or

$$\begin{aligned} PS = & \frac{1}{\mathcal{N}^2} (|CS_+|^2 |w'_1|^2 + |CS_\times|^2 |w'_2|^2 + \\ & + 2\Re(CS_+ \overline{CS_\times}) \Re(w'_1 \bar{w}'_2) + 2\Im(CS_+ \overline{CS_\times}) \Im(w'_1 \bar{w}'_2)) \end{aligned} \quad (22)$$

We see that the power sum is a rational function of coefficients w'_1 and w'_2 . This allows to postpone substitution of these coefficients until after summation is performed. In a typical search the parameters w'_1 and w'_2 should be sampled on a grid containing hundreds of points in order to minimize power loss, thus there is great advantage that only 7 separate sums (4 for the numerator and 3 for the normalizing factor \mathcal{N}) need to be accumulated before substitution.

For convenience we list some common expressions of w'_1 and w'_2 in terms of more conventional parameters ι and ϵ [3, 13–16]:

$$\begin{aligned} w'_1 &= \frac{1+\cos^2(\iota)}{2} \cos(\epsilon) + i \cos(\iota) \sin(\epsilon) \\ w'_2 &= \frac{1+\cos^2(\iota)}{2} \sin(\epsilon) - i \cos(\iota) \cos(\epsilon) \\ |w'_1|^2 &= \frac{1+2\cos^2(\iota)+\cos^4(\iota)}{4} \cos^2(\epsilon) + \cos^2(\iota) \sin^2(\epsilon) \\ |w'_2|^2 &= \frac{1+2\cos^2(\iota)+\cos^4(\iota)}{4} \sin^2(\epsilon) + \cos^2(\iota) \cos^2(\epsilon) \\ \Re(w'_1 \bar{w}'_2) &= \frac{\sin^4(\iota)}{4} \sin(\epsilon) \cos(\epsilon) \\ \Im(w'_1 \bar{w}'_2) &= \frac{1+\cos^2(\iota)}{2} \cos(\iota) \end{aligned} \quad (23)$$

V. ESTIMATION OF INPUT DATA

So far we have assumed that the source signal is bin-centered in the input SFT data $a_{t,f}$. In practice, this is usually not so. Thus the ideal, bin-centered value needs

to be estimated from discretely sampled frequency bins of input SFTs.

To limit contamination from exceedingly steep detector artifacts these SFTs are computed using Hann window which minimizes spectral leakage. We thus need to compute which frequency bins of Hann-windowed SFTs contain putative signal and then devise a linear filter that would estimate signal amplitude in a fractional bin.

In effect, the linear filter thus adds weighted summation of neighboring frequency bins to the quadratic power sum PS . In practice, it is more efficient to compute the estimated fractional frequency bins on discrete grid and then look them up as needed.

A. Hann response function

Consider the function

$$X(t) = Ae^{2\pi i f t} \quad (24)$$

We compute Hann windowed frequency spectrum in bins $\frac{n}{t_1 - t_0}$:

$$\begin{aligned} F_n &= \frac{1}{\sqrt{2\pi}} \frac{1}{t_1 - t_0} \int_{t_0}^{t_1} X(t) \left(1 - \cos\left(2\pi \frac{t - t_0}{t_1 - t_0}\right) \right) e^{-\frac{2\pi i n(t - t_0)}{t_1 - t_0}} dt \\ &= \frac{1}{\sqrt{2\pi}} Ae^{2\pi i f(t_0 + t_1)/2} e^{-\pi i n} \cdot \frac{\sin(\pi \delta)}{\pi \delta(1 - \delta^2)} \end{aligned} \quad (25)$$

where $\delta = f(t_1 - t_0) - n$.

This is an entire holomorphic function of δ which decays as δ^{-3} on the real axis.

Figure 1 shows the plot of F_n without the exponential phase factors. One observes that for practical purposes the function vanishes for $|\delta| > 3$. Indeed, maximum over bins n with $|\delta| > 3$ divided by the value in the bin closest to the injected frequency (and thus with largest F_n) is below 0.01. Power is even more tightly constrained with 99.97% of it occurring in the interval $|\delta| < 2$ (see figure 2).

B. Matched filter estimation of signals at fractional frequency bins

Suppose we have M observations y_i that are linear combinations of signal of unknown strength and noise:

$$y_i = Aa_i + \xi_i \quad (26)$$

here A is the (unknown) amplitude of our signal, a_i are known and ξ_i is the measurement noise.

The goal is to find linear combination $\tilde{A} = \sum_i \beta_i y_i$ with the best signal to noise ratio.

We have:

$$\tilde{A} = A \sum_i \beta_i a_i + \sum_i \beta_i \xi_i \quad (27)$$

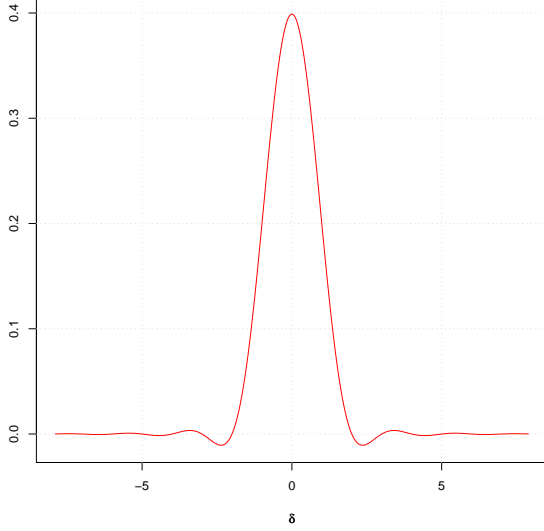


FIG. 1. Amplitude of SFT bin for a test signal mismatched by δ . This is a plot of $\frac{1}{\sqrt{2\pi}} \frac{\sin(\pi\delta)}{\pi\delta(1-\delta^2)}$, excluding exponential phase factors.

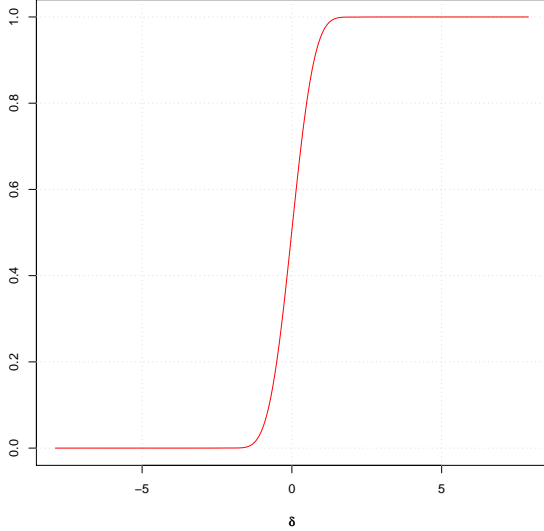


FIG. 2. Integral of $|F_n|^2$, normalized to unity at $+\infty$. This shows total power in SFT bins below $f + \delta$ away from test signal frequency f .

$$\text{SNR} = A \frac{\sum_i \beta_i a_i}{\sqrt{\sum_{i,j} \beta_i \beta_j \langle \xi_i, \xi_j \rangle}} \quad (28)$$

Maximizing SNR is equivalent to minimizing

$\sum_{i,j} \beta_i \beta_j \langle \xi_i, \xi_j \rangle$ while keeping $\sum_i \beta_i a_i$ constant.

Using method of Lagrange multipliers one easily obtains:

$$\sum_j \langle \xi_i, \xi_j \rangle \beta_j = \lambda a_i \quad (29)$$

where λ is an arbitrary, but fixed constant.

Which leads to the well known result:

$$\vec{\beta} = \lambda R^{-1} \vec{a} \quad (30)$$

where $R = |\langle \xi_i, \xi_j \rangle|_{i,j}$. It is usually convenient to pick $\lambda = (\vec{a}^T R^{-1} \vec{a})^{-1}$ - this ensures that a unit signal returns unit response.

For spectrum of Hann windowed signal

$$\xi_i = -\frac{1}{2}\zeta_{i-1} + \zeta_i - \frac{1}{2}\zeta_{i+1} \quad (31)$$

where ζ_i are independent identically distributed Gaussian variables with zero mean. Thus we can assume

$$R_{ij} = \begin{cases} \frac{3}{2} & i = j \\ -1 & |i - j| = 1 \\ \frac{1}{4} & |i - j| = 2 \\ 0 & \text{otherwise} \end{cases} \quad (32)$$

It is instructive to compute R and its inverse for the cases of 5 and 7 SFT bins. For 5 sample points

$$R = \frac{1}{4} \begin{pmatrix} 6 & -4 & 1 & 0 & 0 \\ -4 & 6 & -4 & 1 & 0 \\ 1 & -4 & 6 & -4 & 1 \\ 0 & 1 & -4 & 6 & -4 \\ 0 & 0 & 1 & -4 & 6 \end{pmatrix} \quad (33)$$

$$R^{-1} = \frac{1}{7} \begin{pmatrix} 15 & 20 & 18 & 12 & 5 \\ 20 & 40 & 40 & 28 & 12 \\ 18 & 40 & 52 & 40 & 18 \\ 12 & 28 & 40 & 40 & 20 \\ 5 & 12 & 18 & 20 & 15 \end{pmatrix} \quad (34)$$

For 7 sample points

$$R = \frac{1}{4} \begin{pmatrix} 6 & -4 & 1 & 0 & 0 & 0 & 0 \\ -4 & 6 & -4 & 1 & 0 & 0 & 0 \\ 1 & -4 & 6 & -4 & 1 & 0 & 0 \\ 0 & 1 & -4 & 6 & -4 & 1 & 0 \\ 0 & 0 & 1 & -4 & 6 & -4 & 1 \\ 0 & 0 & 0 & 1 & -4 & 6 & -4 \\ 0 & 0 & 0 & 0 & 1 & -4 & 6 \end{pmatrix} \quad (35)$$

$$R^{-1} = \frac{1}{135} \begin{pmatrix} 336 & 504 & 540 & 480 & 360 & 216 & 84 \\ 504 & 1071 & 1260 & 1170 & 900 & 549 & 216 \\ 540 & 1260 & 1800 & 1800 & 1440 & 900 & 360 \\ 480 & 1170 & 1800 & 2100 & 1800 & 1170 & 480 \\ 360 & 900 & 1440 & 1800 & 1800 & 1260 & 540 \\ 216 & 549 & 900 & 1170 & 1260 & 1071 & 504 \\ 84 & 216 & 360 & 480 & 540 & 504 & 336 \end{pmatrix} \quad (36)$$

This procedure can be used for windows other than Hann, simply by updating matrices R . However, the number of terms and size of the matrices are minimized for Hann-windowed data.

The coefficients a_i can be obtained from the formula 25, however, if we are only interested in computing power $|A|^2$ we can discard the common phase factor depending on f and simplify the formula to

$$a_k = (-1)^k \frac{1}{\sqrt{2\pi}} \cdot \frac{\sin(\pi\delta)}{\pi\delta(1-\delta^2)} \quad (37)$$

where $\delta = f(t_1 - t_0) - k$

VI. DYNAMIC PROGRAMMING METHODS

Search over parameters which cause long-term frequency drift can be made more efficient by use of dynamic programming methods such as Viterbi algorithm [3, 7, 8].

In the simplest implementation, the input data is broken into K chunks. Signal power for a set of frequency bins is computed in each chunk. The power is then accumulated progressively from first to last chunk and at each accumulation stage the power in a frequency bin is replaced by maximum power over a set nearby bins [3].

For example, one can take the maximum over the 3 nearby bins including the central bin. This would allow the frequency path to deviate by as much as $K - 1$ bins. The bin set need not be contiguous or symmetric - this can serve to accommodate large periodic modulation or spindowns.

One issue that arises in practice is that the maximum needs to be taken over power and thus one would need to substitute polarization coefficients into the power sum. When the grid of sampled polarization is not carefully controlled the amount of computation can be large enough to be comparable (or even dominate) the computation of the loosely coherent sum.

As common to a dynamic programming algorithm the memory requirements for efficient computation can be large as well.

Ideally, the maximum should be computed at the power sum level before substituting polarization coefficients. However, the exact implementation is difficult because the maximum of two quadratic forms or two rational functions is in general a *piecewise* rational function.

This difficulty could be overcome by replacing the piecewise function with a rational function that majorates it - i.e. yields power greater than what would be produced by the exact computation. This gives up some sensitivity for an increase in computational efficiency.

VII. IMPLEMENTATION TESTING

A. Execution speed

Algorithmic improvements tend to have the largest impact on software performance. This is because code optimization usually speeds up a section of the code by at most few hundred percent and the speedup is constant over computation scale. In some situations, such optimization loses with scale as limited hardware features are exhausted when scaling parameter is increased.

In contrast, an algorithm with smaller power of scaling parameter in asymptotic running time will gain performance with increase in the scaling parameter.

However, sometimes computational hardware is not suitable for a particular algorithm. For example, contemporary CPUs typically do not have dedicated instructions for modular arithmetic, or vector based sorting primitives.

In addition, an actual search has to deal with large numbers of outliers, limited storage and other issues affecting algorithm suitability.

This makes quantitative comparison of algorithms rather tricky. Ideally, we would want the implementation of each algorithm to be done in the best way possible and the execution conditions to mimic actual search. It seems reasonable to allow optimizing compilers to rearrange code, but, strictly speaking, this changes the algorithm.

To illustrate that the algorithm described in this paper is suitable for contemporary computing hardware we present a comparison with previous loosely coherent implementation. Due to caveats discussed above one should not take this as an actual measure of a speedup in a real search.

Both algorithms were compiled into the same executable using gcc 6.3.0 compiler and used exactly the same optimization flags. They were both run on O1 1800s Hann-windowed SFTs and analyzed the same frequency range 200-200.125 Hz. The execution node had ample memory and 32 simultaneously executing threads on Intel Xeon E5-2620 processors.

To save execution time the analysis was restricted to 0.5 rad disk around Right Ascension 0 and declination 0.

The results are shown in table I. The previous loosely coherent code refers to the loosely coherent implementation used in [2, 3, 10]. The column for the new loosely coherent code refers to the implementation of the algorithm described in this paper.

The previous loosely coherent code used phase tolerance as a parameter and a Lanczos window for the kernel. Because of this, the coherence length is only approximate as the SFTs that took part in the coherent sum were combined with different weights and the window tails covered 43200 seconds of data.

The coherence length for the new algorithm is better defined, with distance between start of SFTs limited to 14400s. Note that because of Hann-windowing the co-

Parameter	Previous loosely coherent code	New loosely coherent code
Coherence length (s)	~ 14400	14400
Phase tolerance (rad)	$\pi/8$	NA
Data load time (s)	82	87
Total running time (s)	2579	285
Inner loop time (s)	2497	198
Upper limit	4.25e-25	3.75e-25

TABLE I. Execution speed

Execution speed of loosely coherent algorithms. The new implementation is faster and uses the data more efficiently producing smaller upper limits.

herent sum made use of data points more than 16000s but with progressively smaller weights near the ends of the window.

In addition, both codes used real data with duty cycle less than 100%. Thus some coherent sums simply did not have enough data to fill the entire coherence sum.

The upper limit quoted in the table is the worst-case upper limit on all points searched in the grid. The worst-case is typically reached for linear polarizations which introduce strong modulation on SFT weights with approximately 12 hour period. This further decreases effective coherence length, but the effect is similar for both algorithms.

The data load time describes the time to load all the input time and to perform initialization of all data structures. Total running time describes actual wall-clock time for each code. In the actual application the work load is usually sized to be much larger than input time.

The inner loop time is the difference between total running time and data load time. It includes the time spent running loosely coherent algorithms as well as the time spent in post-processing their results. The postprocessing algorithm was the same in both instances.

We observe more than 10x improvement in running time, while the upper limit is smaller by 12%. We note that if the phase tolerance parameter was further reduced for the previous loosely coherent code the upper limit would improve, but the running time will greatly increase.

B. Validation

In this section, we describe validation of the software pipeline implemented using medium scale *Loosely coherent* algorithm using Monte-Carlo injections. This demonstrates that the *Loosely coherent* algorithm can be implemented on modern hardware and it is practical for searches of disks on the sky. Upcoming papers will describe search results.

The analysis pipeline follows the method described in [2, 3]. The practical implementation is a pipeline that progressively increases coherence length (Table II). Each stage, except the last, identifies templates with large upper limits and SNR and writes their parameters to file.

Stage	Coherence length (hours)	Minimum SNR
0	8	6
1	12	6.5
2	16	7
3	24	8
4	36	9
5	48	11
6	72	13

TABLE II. Simulation parameters

Parameters of 6-stage pipeline used for simulations. Stage 6 outliers are subjected to consistency check between interferometers.

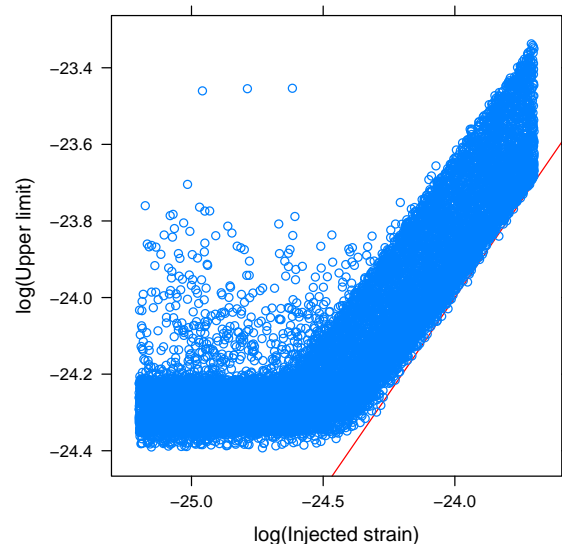


FIG. 3. Established upper limit versus injection strength.

These templates are excluded from computation of stage-specific aggregate quantities such as maximum upper limit and SNR. The followup stage analyses templates from the file produced by previous stage.

At the last stage the analysis is done twice - using coherent combination of interferometers and also separately for each interferometer. All outliers are written into the

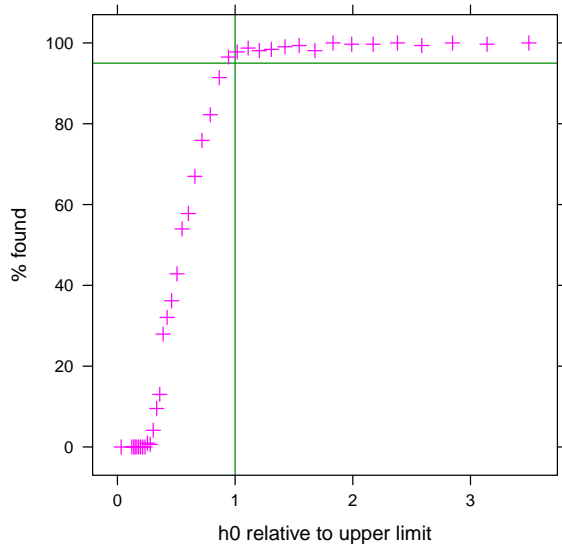


FIG. 4. Fraction of injections that had a nearby outlier at the end of the 6-stage pipeline. The X-axis of this figure shows ratio of injection strain to the no-injection upper limit. The Y-axis shows percentage of correctly detected injections. This meant that the injection had to have an outlier nearby that passed all analysis stages. The horizontal green line is drawn at 95% level.

file. The threshold for outlier SNR from individual interferometers is set at 6. A consistency check is applied, requiring outliers from coherent combination of interferometers to match outliers from individual interferometers in frequency, sky and spindown.

The pipeline was tested with software injections into O1 data [17] from Advanced LIGO interferometers [18]. The O1 run occurred between September 12, 2015 and January 19, 2016.

The injections were done randomly into the range of 975-1500 Hz into a disk on the sky of radius 0.06 rad (3.43°) centered on Right Ascension 4.65 rad (266.42°) and declination -0.46 rad (-26.35°). The disk was chosen to cover the center of our galaxy. The spindown of the injections was logarithmically distributed between -5.7×10^{-12} and -1.8×10^{-10} .

The upper limits are computed as a maximum of upper limits from every stage. Figure 3 shows results of simulation covering range 975-1500 Hz, where injections were performed into a region near galactic center. The 95% confidence level upper limits are correctly established, with most points above the red diagonal line. The three outlier points and the scatter of high upper limits for small injection strengths are due to detector artifacts [2, 3].

Figure 4 shows detection efficiency of the pipeline. The X-axis of this figure shows ratio of injection strain to the no-injection upper limit. This upper limit is established

in a small sky area (disk with 0.02 rad radius) around the injection location by the first stage of the pipeline. In a real search the upper limits are computed as a maximum over larger parameter space, which would shift the X-axis to the right.

The Y-axis of figure 4 shows fraction of injections that had a nearby outlier. This outlier had to have an SNR of at least 13, be within $15 \mu\text{Hz}$ of true injection frequency and within 1.5×10^{-11} Hz/s of true injection spindown.

In addition, nearby outliers had to be no further than $6.5 \times 10^{-4} \cdot (1 \text{ kHz}/f)$ in ecliptic distance, defined as the distance between outlier location and true injection location after projection onto the ecliptic plane. Here f is the outlier frequency.

Because high-SNR outliers are passed to subsequent stages we retain ability to make detection below the upper limit established by the first stage. Thus the effective coherence length of the pipeline is larger than the length defined by the first stage.

VIII. CONCLUSIONS

We have described a new *Loosely coherent* algorithm for medium scale coherence lengths. Simulations of a full pipeline incorporating this algorithm have been demonstrated on O1 data [17, 19] from Advanced LIGO interferometers [18].

Compared with previous implementation, more than 10x improvement in computational speed has been observed.

The new pipeline allows all-sky loosely coherent analysis for the first time, extending reach of wide-parameter searches for continuous gravitational wave signals.

IX. ACKNOWLEDGMENTS

The simulations were performed on ATLAS cluster at AEI Hannover. We thank Carsten Aulbert and Henning Fehrmann for their support.

The author thanks the LIGO Scientific Collaboration for access to the data and gratefully acknowledge the support of the United States National Science Foundation (NSF) for the construction and operation of the LIGO Laboratory and Advanced LIGO as well as the Science and Technology Facilities Council (STFC) of the United Kingdom, and the Max-Planck-Society (MPS) for support of the construction of Advanced LIGO. Additional support for Advanced LIGO was provided by the Australian Research Council.

This research has made use of data, software and/or web tools obtained from the LIGO Open Science Center (<https://losc.ligo.org>), a service of LIGO Laboratory, the LIGO Scientific Collaboration and the Virgo Collaboration. LIGO is funded by the U.S. National Science Foundation. Virgo is funded by the French Centre National de Recherche Scientifique (CNRS), the Italian

Istituto Nazionale della Fisica Nucleare (INFN) and the Dutch Nikhef, with contributions by Polish and Hungar-

ian institutes.

We also thank the anonymous referees for many useful comments.

-
- [1] First low-frequency Einstein@Home all-sky search for continuous gravitational waves in Advanced LIGO data, B. P. Abbott *et al.* (LIGO Scientific Collaboration and Virgo Collaboration), *Phys. Rev. D* **96** 122004 (2017)
 - [2] All-sky search for periodic gravitational waves in the O1 LIGO data, B. P. Abbott *et al.* (LIGO Scientific Collaboration and Virgo Collaboration), *Phys. Rev. D* **96** 062002 (2017).
 - [3] Full Band All-sky Search for Periodic Gravitational Waves in the O1 LIGO Data, B. P. Abbott *et al.* (LIGO Scientific Collaboration and Virgo Collaboration), *Phys. Rev. D* **97** 102003 (2018).
 - [4] On blind searches for noise dominated signals: a loosely coherent approach, V. Dergachev, *Class. Quantum Grav.* **27**, 205017 (2010).
 - [5] Data analysis of gravitational-wave signals from spinning neutron stars. I. The signal and its detection. P. Jaranowski, A. Królak, and B. F. Schutz, *Phys. Rev. D* **58**, 063001 (1998).
 - [6] Extraction of Signals from Noise, L. A. Wainstein, V. D. Zubakov (1971)
 - [7] Error bounds for convolutional codes and an asymptotically optimum decoding algorithm, A. Viterbi, *IEEE Transactions on Information Theory* **13**, 260 (1967).
 - [8] Search for gravitational waves from Scorpius X-1 in the first Advanced LIGO observing run with a hidden Markov model, B.P. Abbott *et al.* (LIGO Scientific Collaboration and Virgo Collaboration), *Phys. Rev. D* **95**, 122003 (2017)
 - [9] Efficient Estimation of Barycentered Relative Time Delays for Distant Gravitational Wave Sources Orion Sauter, Vladimir Dergachev, Keith Riles, arXiv:1712.06118 [astro-ph.IM]
 - [10] A search of the Orion spur for continuous gravitational waves using a "loosely coherent" algorithm on data from LIGO interferometers J. Aasi *et al.* (LIGO Scientific Collaboration and Virgo Collaboration), *Phys. Rev. D* **93**, 042006 (2016).
 - [11] Loosely coherent searches for sets of well-modeled signals, V. Dergachev, *Phys. Rev. D* **85**, 062003 (2012)
 - [12] The cubic algorithm, E. Galperin, *Journal of Mathematical Analysis and Applications* **112**, 2, (1985)
 - [13] All-sky search for periodic gravitational waves in LIGO S4 data, B. Abbott *et al.* (LIGO Scientific Collaboration), *Phys. Rev. D* **77**, 022001 (2008).
 - [14] All-sky LIGO Search for Periodic Gravitational Waves in the Early S5 Data, B. P. Abbott *et al.* (LIGO Scientific Collaboration), *Phys. Rev. Lett.* **102**, 111102 (2009).
 - [15] All-sky Search for Periodic Gravitational Waves in the Full S5 Data, B. Abbott *et al.* (The LIGO and Virgo Scientific Collaboration), *Phys. Rev. D* **85**, 022001 (2012).
 - [16] Comprehensive All-sky Search for Periodic Gravitational Waves in the Sixth Science Run LIGO Data J. Aasi *et al.* (LIGO Scientific Collaboration and Virgo Collaboration), *Phys. Rev. D* **94**, 042002 (2016).
 - [17] LIGO Open Science Center, <https://losc.ligo.org>
 - [18] Advanced LIGO, J. Aasi *et al.* (LIGO Scientific Collaboration), *Class. Quantum Grav.* **32** 7 (2015)
 - [19] M. Vallisneri *et al.* "The LIGO Open Science Center", proceedings of the 10th LISA Symposium, University of Florida, Gainesville, May 18-23, 2014, arXiv:1410.4839